Journal of Porphyrins and Phthalocyanines
J. Porphyrins Phthalocyanines 2001; **5**: 289–299

Status of theoretical modeling of tautomerization in free-base porphyrin

DILIP K. MAITY† and THANH N. TRUONG*

Henry Eyring Center for Theoretical Chemistry, Department of Chemistry, University of Utah, Salt Lake City, UT 84112, USA

Received 10 October 1999
Accepted 18 March 2000

ABSTRACT: We provide a review on the status of theoretical modeling of tautomerization in free-base porphyrin. We focus our discussion on several aspects, namely: (1) potential surfaces for both the stepwise and concerted mechanisms calculated at different levels of theory, (2) solvent effects and (3) kinetics. The importance of quantum mechanical tunneling in this double hydrogen atoms transfer process is analyzed. Copyright © 2001 John Wiley & Sons, Ltd.

KEYWORDS: mechanism; kinetics; direct dynamics; variational transition state theory; tunneling; porphyrin; hydrogen migration; tautomerization

INTRODUCTION

Porphyrins are known to play important roles in many fundamental biological processes, e.g. photosynthesis, metal coordination chemistry, biological redox reactions and oxygen transport processes [1]. Since porphyrins posses large extended π-electron systems and have high stability, they are finding use in advanced materials as components in organic metals, molecular wires and other devices for electronics and optoelectronics [2]. Because of their photodynamic therapeutic behavior, porphyrins are also being used in medicine for the treatment of cancer and dermatological diseases [2, 3]. Free-base porphyrin has two hydrogen atoms in the inner part of the skeleton and it is known that the inner hydrogen atoms migrate in a framework of four nitrogen sites. This double hydrogen atoms transfer process in free-base porphyrin is also known as NH tautomerization. Due to the biological and potential technological applications, an understanding of the mechanism of the inner-hydrogen tautomerization process in free-base porphyrin is of significant importance. For this reason, it has drawn attention in much theoretical [4–24] and experimental [25–50] research. A detailed understanding of this tautomerization process is a gateway for understanding the mechanism of metal insertion into porphyrins. Theoretical chemistry has played a significant role in understanding the mechanism of this process, providing molecular-level information that is difficult to obtain by experimental means. Unfortunately, to date there are many scattered theoretical reports on different aspects of the NH tautomerization. The aim of this review is to provide an up-to-date comprehensive picture on the progress of theoretical modeling of this important tautomerization process.

There are two main issues regarding NH tautomerization, namely mechanism and kinetics. The following section is devoted to discussion on the mechanism aspect, i.e. the potential energy surface, which is the focus of most theoretical studies. This includes an important issue that is already resolved, namely, the stepwise versus concerted reaction pathways, and new results on solvent effects and structural changes along the preferred reaction path. The kinetic aspect of the NH tautomerization process is presented in the kinetics section. Very little theoretical studies were done in this direction. In fact, there were only three studies to date [21, 24, 51]. We will elaborate more on the recent results on the importance of quantum mechanical tunneling and their effects on the observed activation energy. Finally, in the conclusion section we provide some discussion on the new challenge on the theoretical study of NH tautomerization in free-base prophyrin.

POTENTIAL ENERGY SURFACE

Early experimental evidence from X-ray studies [25, 48] indicates that the crystal structure of free-base porphyrin is not unambiguous. There is an uncertainty about the molecular symmetry point group of the most stable *trans* isomer as to whether it is of C_{2v} or D_{2h} symmetry. These studies also found no direct evidence for the existence of the *cis* isomer. More recent NMR studies [33, 50] suggests a high symmetry structure with nearly equivalent carbon–carbon bonds. As discussed below, the recent experimental and theoretical results confirm that the *trans* isomer has D_{2h} symmetry. Solid state NMR studies [49] indicate a fast tautomerization between *trans* and *cis* isomers at room

*Correspondence to: T. N. Truong, Henry Eyring Center for Theoretical Chemistry, Department of Chemistry, University of Utah, 315 S 1400 E Room Dock, Salt Lake City, UT 84112, USA.
† On leave from Chemistry Division, Bhabha Atomic Research Centre, Bombay, India.

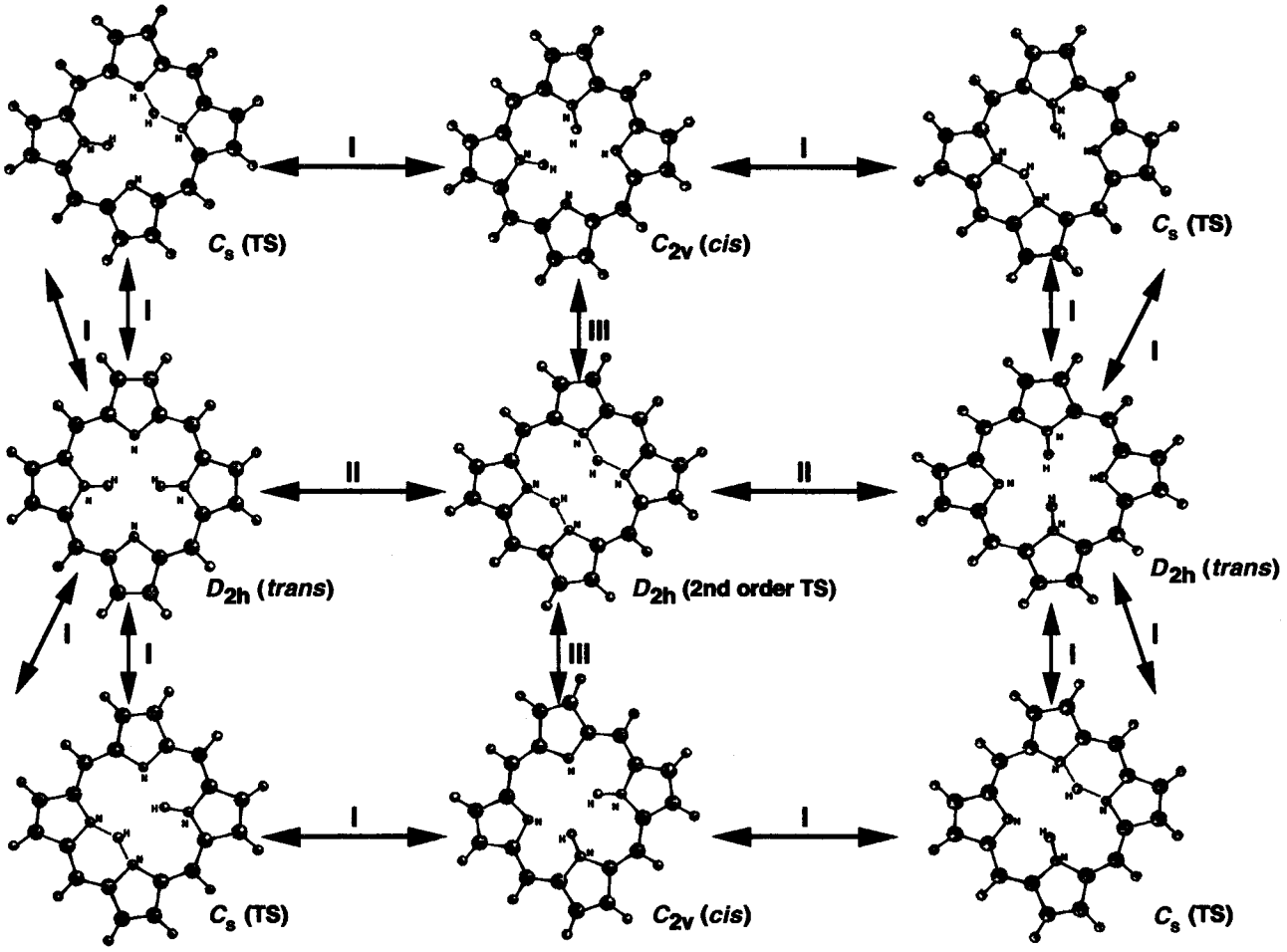

Fig. 1. Schematic diagram of the inner-hydrogen tautomerization process of free-base porphyrin. The path for the stepwise mechanism is labeled I and that for the concerted mechanism is labeled II. The path III connects the second-order saddle-point geometry to the intermediate geometry. The symmetry of each stationary point geometry is also shown.

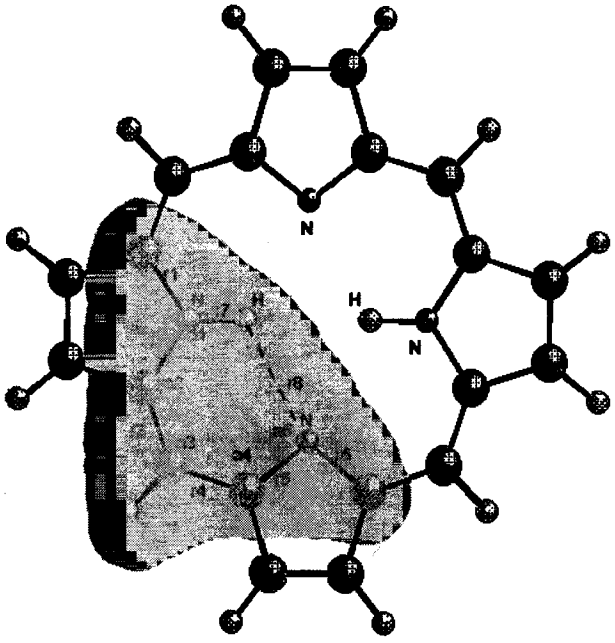

Fig. 2. Calculated structure for the D_{2h} *trans*-isomer. The shaded area shows the model system for the present integrated MO + MO (IMOMO) calculations and capped hydrogen atoms. See Table 1 for calculated experimental values of selected bond distances and bond angles at different levels of theory.

temperature. There are two proposed mechanisms for the NH tautomerization process, namely, stepwise [10, 26, 37, 39, 40] and concerted [6, 11, 12, 27, 28]. The stepwise mechanism where the two hydrogen atoms migrate one after another as shown in path I of Fig. 1 is characterized by a *trans–cis–trans* conversion with the *trans*-isomer as the reactant and the *cis*-isomer as the metastable intermediate. The concerted mechanism involves synchronous migration of the two hydrogen atoms as shown in path II of Fig. 1. The debate as to whether the mechanism is stepwise or concerted extends back many years for both experiment and theory. It is now proven both theoretically [9, 11, 13, 16–21, 24] and experimentally [38, 39, 41, 42, 49] that the double proton transfer occurs via a two-step mechanism involving a metastable *cis* intermediate rather than by a synchronous one-step path. In the following subsections we provide different aspects of potential energy surface studies to provide insights into the mechanism of NH tautomerization.

Structures and Frequencies

Early attempts on theoretical studies on the structure of free-base porphyrin were limited to semiempirical molecular orbital (MO) and Hartee–Fock methods with small basis sets. With the recent advancement of computer technology, density functional theory (DFT) and correlated *ab initio* MO calculations become possible. Depending on the quality of

Table 1. Calculated and experimental values of selected bond distances and bond angles for the stable *trans*-isomer (D_{2h}). Bond distances are in ångströms and bond angles are in degrees. See Fig. 2 for labels of bond lengths and angles

Bond length (r)/ bond angle (a)	BH&HLYP[a]	LDA[b]	B3LYP/TZ2P[c]	X-ray[d]
r1	1.36	1.36	1.37	1.38
r2	1.36	1.36	1.37	1.38
r3	1.38	1.39	1.39	1.40
r4	1.39	1.39	1.39	1.37
r5	1.35	1.36	1.36	1.38
r6	1.35	1.36	1.36	1.39
r7	1.00	1.04	1.01	0.86
r8	2.29	–	2.31	–
a1	124.6	125.1	124.6	129.0
a2	125.7	126.2	125.6	125.0
a3	126.8	127.6	127.1	126.5
a4	125.7	124.3	125.6	125.6
a5	98.7	–	98.6	–

[a] Ref. [24].
[b] Ref. [18].
[c] Ref. [21].
[d] Ref. [25].

the wave function, different results were obtained. In particular, both semiempirical [52] and *ab initio* HF methods [13] yielded a symmetry broken C_{2v} structure for the *trans* isomer. Inclusion of electron correlation at the MP2 level yields the higher symmetry (D_{2h}) structure [13]. This prediction has also been verified using multi-reference configuration interaction (CI) wave functions and non-local hydrid density functional B3LYP [21] and BH&HLYP [24] calculations and is consistent with the experimental data [4, 16–19, 43–48]. The structure of the *trans* isomer is depicted in Fig. 2. For comparisons on the performance of different methods, calculated geometrical parameters are listed in Table 1 along with experimental data. Note that the calculated geometrical data using the BH&HLYP [24] B3LYP [21] and LDA [14] methods are quite similar with the largest differences of 0.04 Å in bond length and 1.4° in bond angles. The LDA bond length of 1.04 Å for the NH bond (r7) is noticeably longer than that from the non-local hybrid B3LYP, BH&HLYP or MP2 calculations. Theoretical predictions in general agree well with X-ray data [25]. The largest differences between calculated and X-ray structures are 0.18 Å in bond lengths (N–H bond, r7) and 5.6° in bond angles (∠CNH angle, a1). However, it has been pointed out earlier that X-ray methods are not able to locate hydrogen nuclei accurately and the estimated N–H bond distance of 0.86 Å by the X-ray method is certainly too short compared to the normal N–H bond. The theoretical vibrational spectrum of the *trans* isomer has also been reported using a scaled quantum mechanical force field based on the B3LYP/6-31G* force constants. The agreement between the calculated and experimental frequencies is quite good with the mean deviation being 5 cm^{-1} [20]. For the *cis*-isomer with structure shown in Fig. 3, a few selected important geometrical parameters are listed in Table 2. Note that the BH&HLYP [24] optimization was done without any symmetry constraint, whereas B3LYP [21] and LDA [14] calculations used C_{2v} symmetry constraint. Similar to the *trans*-isomer, the LDA N–H (r8) bond length of the *cis*-isomer is 1.06 Å too long while the ∠CNH angle (a5) is 115.3° too short compared to that of non-local hybrid B3LYP or BH&HLYP calculations. Again

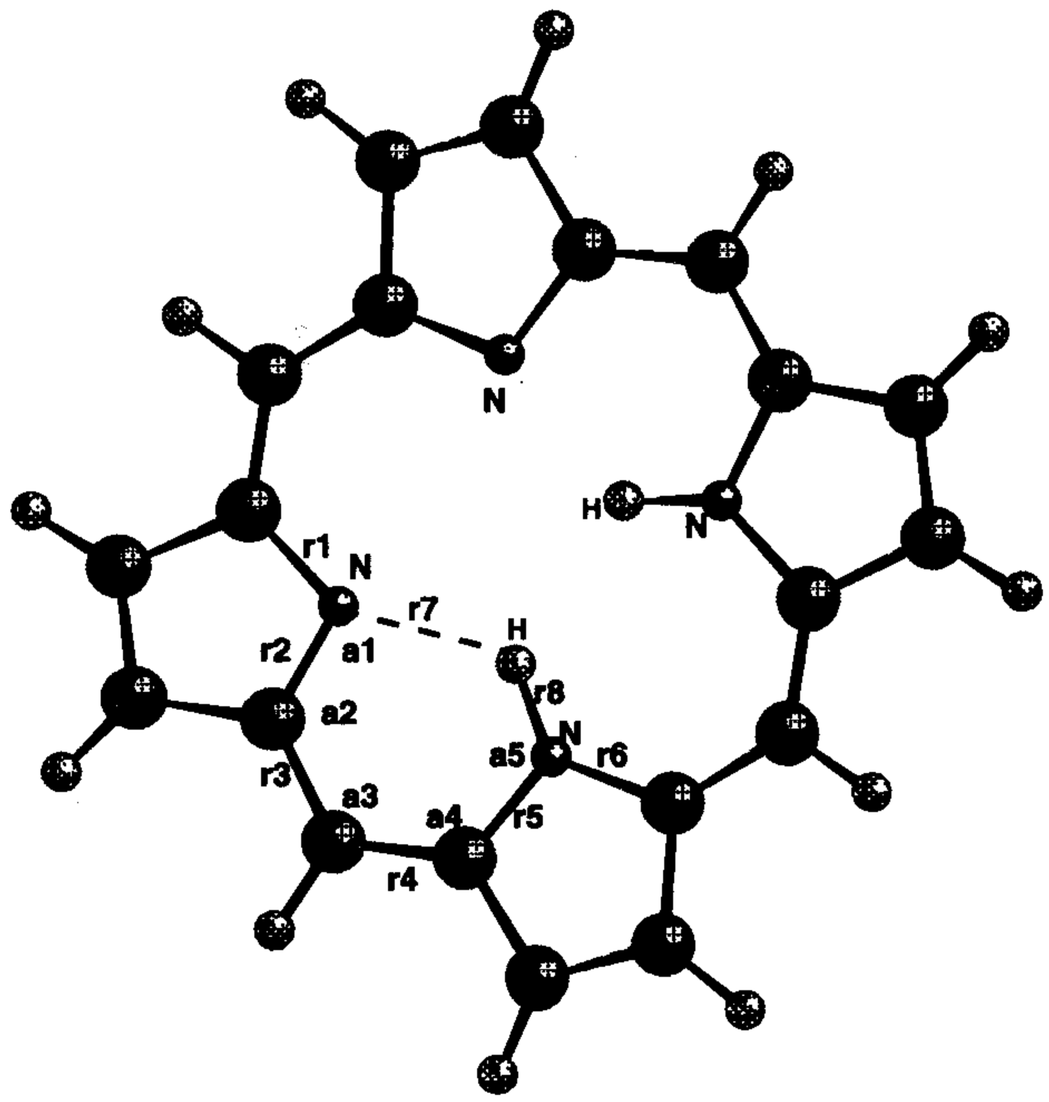

Fig. 3. Calculated structure for the C_{2v} *cis*-isomer. See Table 2 for calculated values of selected bond distances and bond angles at different levels of theory.

Table 2. Calculated values of selected bond distances and bond angles for the metastable *cis*-isomer (C_{2v}). Bond distances are in ångströms and bond angles are in degrees. See Fig. 3 for labels of bond lengths and angles

Bond length (r)/ bond angle (a)	BH&HLYP[a]	LDA[b]	B3LYP/TZ2P[c]
r1	1.34	1.36	1.35
r2	1.35	1.36	1.36
r3	1.39	1.39	1.40
r4	1.38	1.39	1.39
r5	1.36	1.37	1.37
r6	1.36	1.37	1.35
r7	1.94	–	1.94
r8	1.01	1.06	1.02
a1	101.8	–	101.7
a2	123.2	122.5	123.1
a3	124.0	123.4	124.2
a4	123.6	122.5	123.3
a5	117.7	115.3	117.3

[a] Ref. [24].
[b] Ref. [18].
[c] Ref. [21].

Table 3. Calculated values of selected bond distances and bond angles for the transition state (C_s). Bond distances are in ångströms and bond angles are in degrees. See Fig. 4 for labels of bond lengths and angles

Bond length (r)/ bond angle (a)	BH&HLYP[a]	B3LYP/TZ2P[b]
r1	1.36	1.37
r2	1.36	1.37
r3	1.38	1.39
r4	1.38	1.39
r5	1.36	1.37
r6	1.36	1.35
r7	1.32	1.33
r8	1.28	1.29
a1	105.8	105.6
a2	121.1	121.1
a3	120.4	120.9
a4	121.6	121.5
a5	105.8	105.6

[a] Ref. [24].
[b] Ref. [21].

showing very small differences in the results obtained from BH&HLYP and B3LYP optimization. Using the same scaled quantum mechanical force field factor as in the case of the *trans*-isomer, Baker and co-workers have suggested the IR active mode at 2333 cm^{-1} to be the 'fingerprint' for detecting the *cis*-isomer in the presence of the more stable *trans*-isomer.

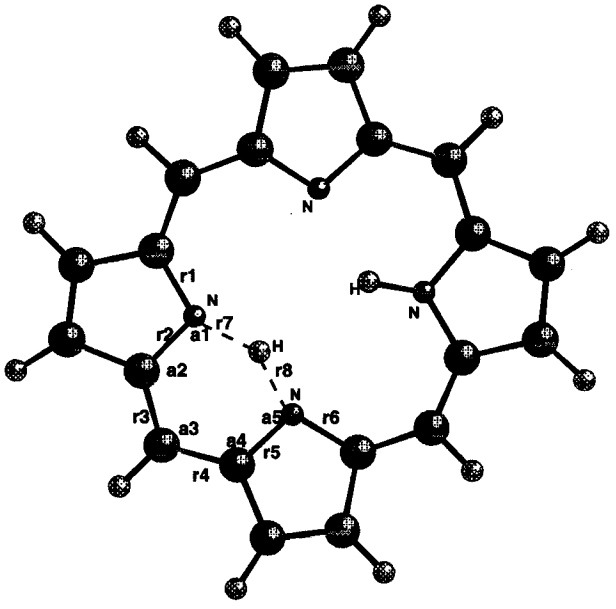

Fig. 4. Calculated structure of C_s transition state. See Table 3 for calculated values of selected bond distances and bond angles at different levels of theory.

An initial effort to characterize the transition state structure for the stepwise mechanism at a correlated level was undertaken by Reimers *et al.* [17] using a partial optimization procedure at the MP2 level of theory. Recently, B3LYP/6-31G(d) [21] and BH&HLYP/6-31G(d,p) [24] methods have also been applied to optimize the transition state structure with C_s symmetry constraint. Normal mode analyses were performed to confirm the saddle point structure to having C_s symmetry with a single imaginary frequency of 1671 $i\,cm^{-1}$ and 1583 $i\,cm^{-1}$ at the B3LYP and BH&HLYP levels of theory, respectively. These values can be compared to the experimental estimate of 1425–1853 $i\,cm^{-1}$ [41]. The structure of the stepwise transition state is shown in Fig. 4, and a few selected geometrical parameters calculated at B3LYP and BH&HLYP levels of theory are listed in Table 3. Similarly, the differences between the B3LYP and BH&HLYP results are very small. Both methods predict that the transferring hydrogen atom lies closer to the accepting nitrogen by 0.04 Å, indicating that this transition state is closer to the intermediate structure as intuitively predicted from the reaction energy of tautomerism in accordance with Hammond's postulate [53]. The second-order transition state structure of the concerted mechanism has been optimized with D_{2h} symmetry constraints at the RHF [17] B3-LYP/6-31G(d) [21] and BH&HLYP/6-31G(d,p) [24] levels of theory. The structure for this transition state is depicted in Fig. 5, and a few selected geometrical parameters calculated at B3LYP and BH&HLYP levels of theory are listed in Table 4. The largest differences between the calculated bond distances and bond angles between

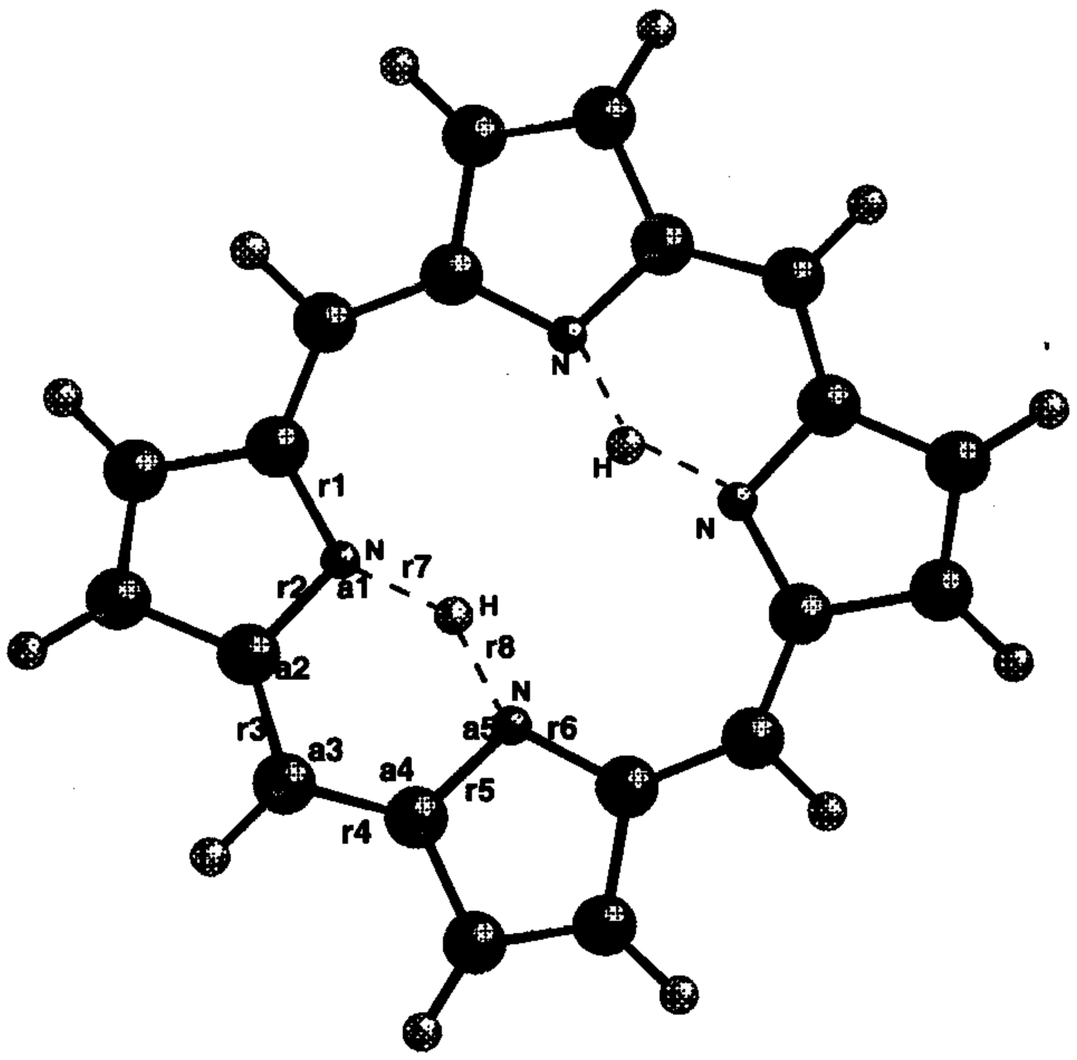

Fig. 5. Calculated structure for the D_{2h} second-order saddle point. See Table 4 for calculated values of selected bond distances and bond angles at different levels of theory.

these two DFT methods are 0.02 Å and 0.5°, respectively. BH&HLYP normal mode analysis yielded two imaginary frequencies of 1654 *i* and 1562 *i* cm^{-1} compared to those of 1853 *i* and 1425 *i* cm^{-1} from the B3LYP calculations. Maity *et al.* [24] pointed out that the eigenvector of the smaller imaginary frequency shows motions of the two hydrogen atoms moving in the same direction. This motion corresponds to the path that connects the second-order saddle point and the *cis*-isomer as denoted by reaction path III in Fig. 1. Opposite movement of the two hydrogen atoms corresponds to the larger imaginary frequency mode. This movement connects the two *trans*-isomers (reactant) on the potential energy surface and is denoted by reaction path II in Fig. 1.

Energetics

Calculated reaction energies, i.e. the energy difference between the *trans*- and *cis*-isomers, and barrier heights along with the experimental estimates are listed in Table 5. In an attempt to improve the energetic information of the stepwise mechanism, single-point energy calculations were done [24] using the IMOMO methodology recently proposed by Morokuma and co-workers [54]. This method has shown to provide rather accurate energetic information compared to full high-level calculations but at a significantly less cost particularly for large systems such as porphyrins. In these calculations, a small active sub-region as shown in the shaded region of Fig. 2, that is most critical to the chemical process, is treated at the more accurate CCSD(T)/cc-pVDZ level of theory while the remaining region is still at the BH&H/6-31G(d,p) level of theory. Reaction energies are calculated in the range of 7.6–10.0 kcal mol^{-1}. Interestingly, the MP2 energy on LDA geometry is the lower bound and the MP2 energy on RHF geometry is seen to be the upper bound. The BH&HLYP method predicted the energy difference between the reactant (*trans*-isomer) and intermediate (*cis*-isomer) to be 9.1 kcal mol^{-1} and is 0.8 kcal mol^{-1} larger than the B3LYP value. IMOMO- B3LYP- and MP2-predicted classical barrier heights for the *trans–cis* tautomerization process are in good agreement with the upper limit of the experimental estimate range for the classical barrier height of 12.6–16.3 kcal mol^{-1} (from a laser induced fluorescence spectroscopic measurement [41]. The BH&HLYP barrier is about 2 kcal mol^{-1} too high compared to other theoretical results. The reverse classical barrier height for the *trans–cis* tautomerization (the barrier height for the second step of tautomerization) process in the stepwise mechanism is calculated to be 9.9, 9.5 and 8.7 kcal mol^{-1} at the B3LYP, BH&HLYP and IMOMO levels, respectively. However, the classical barrier height for the concerted mechanism is calculated to be smaller by ~3 kcal mol^{-1} following BH&HLYP than B3LYP and by ~2 kcal mol^{-1} larger than the MP2 method. Zero-point energy corrections were found to change the energy difference between reactant and intermediate by only 0.4 kcal mol^{-1}, while lower the classical barriers in both mechanisms by about 3 kcal mol^{-1}. All the methods predict the concerted mechanism to have a higher barrier than that of the stepwise mechanism by several kcal mol^{-1}.

Table 4. Calculated values of selected bond distances and bond angles for the second-order saddle point (D_{2h}) structure. Bond distances are in ångströms and bond angles are in degrees. See Fig. 5 for labels of bond lengths and angles

Bond length (r)/ bond angle (a)	BH&HLYP[a]	B3LYP/TZ2P[b]
r1	1.35	1.36
r2	1.36	1.37
r3	1.38	1.39
r4	1.38	1.39
r5	1.36	1.37
r6	1.35	1.36
r7	1.28	1.30
r8	1.28	1.30
a1	106.7	106.5
a2	120.9	120.9
a3	120.0	120.5
a4	120.9	120.9
a5	106.8	106.5

[a] Ref. [24].
[b] Ref. [21].

Effects of Solvents

To obtain an estimate for the solvent effects on the reaction energetics of this tautomerization process, Maity *et al.* [24] have performed single-point energy calculations for stationary point structures in different solvents using the Polarizable Continuum Model (PCM) [55] at the BH&HLYP/6-31G(d,p) level of theory. In particular,

Table 5. Calculated reaction energy ΔE classical barrier height $\Delta V^{\ddagger}$ and zero-point energy corrected barrier height ΔV_a for the inner hydrogen atom transfer process in free-base porphyrin in kcal mol^{-1}

Study	ΔE	$\Delta V^{\ddagger}$	ΔV_a
Semi-empirical[a]	8.9		
MP2/DZP//RHF SCF/DZP[b]	10.0		
MP2//LDF[c]	7.6		
B3-LYP/TZ2P[d]	8.3		
BH&HLYP/6-31G(d,p)[e]	9.1		
IMOMO(CCSD(T):BH&HLYP)[e]	8.2		
Stepwise mechanism:			
trans → ts			
Butenhoff and Moore[f]		12.6–16.3[g]	
MP2/DZP//RHF SCF/DZP[b]		16.7	
B3LYP/TZ2P[d]		16.2	13.1
BH&HLYP/6-31G(d,p)[e]		18.6	15.6
IMOMO(CCSD(T):BH&HLYP)[e]		16.9	
cis → ts			
B3LYP/TZ2P[d]		9.9	5.0
BH&HLYP/6-31G(d,p)[e]		9.5	6.8
IMOMO(CCSD(T):BH&HLYP)[e]		8.7	
Concerted mechanism:			
trans → ts			
MP2/DZP//RHF SCF/DZP[b]		19.3	
B3LYP/TZ2P[d]		24.4	18.3
BH&HLYP/6-31G(d,p)[e]		21.6	17.1

[a] Ref. [7].
[b] Ref. [17].
[c] Ref. [18].
[d] Ref. [21].
[e] Ref. [24].
[f] Ref. [41].
[g] This is an experimental study.

heptane (dielectric constant, $\varepsilon = 1.92$), toluene ($\varepsilon = 2.38$) and ethanol ($\varepsilon = 24.55$) were chosen for such calculations as these solvents were often used in the experimental studies. The calculated reaction energy difference between the *trans*- and *cis*-isomers, and classical barrier heights are displayed in Table 6. For non-polar solvents such as heptane and toluene, solvent effects on the reaction energy difference and barrier height are negligible. The effect is slightly larger for polar solvents such as ethanol. Note that an increase of about 1 kcal mol^{-1} in the barrier height due to ethanol solvent results from a small solvation free energy of the transition state structure as compared to those of the reactant or intermediate. The small calculated solvent effects support the earlier experimental report on the solvent independence of the rate of intra-molecular hydrogen atom transfer in free-base porphyrin [27]. It has also been observed from liquid and solid NMR studies that this NH tautomerization behavior is the same in liquid solution and in bulk solid indicating the absence of medium influence [56]. This also implies that gas-phase calculations as done by Baker *et al.* [21] and Maity *et al.* [24] are sufficient to study the inner hydrogen transfer process in the free-base porphyrin system.

Table 6. Comparison of calculated BH&-HLYP/6-31G(d,p) reaction energies, ΔE, and classical barrier heights, $\Delta V^{\ddagger}$ (kcal mol^{-1}), in the gas phase and different solvents for the NH tautomerization process in free-base porphyrin

Solvent	ΔE	$\Delta V^{\ddagger}$
Gas phase	9.1	18.6
Heptane	9.5	18.9
Toluene	9.0	18.8
Ethanol	8.6	19.7

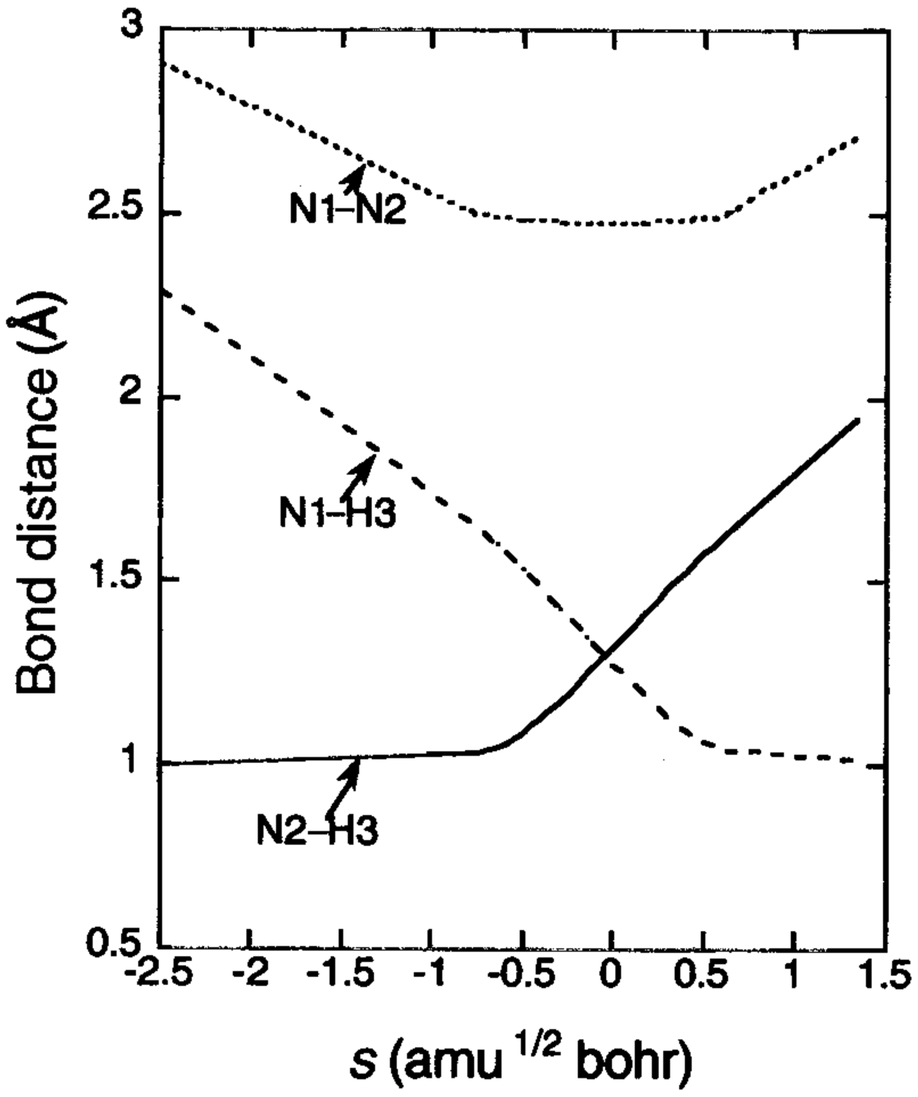

Fig. 6. Selected bond distance profiles along the minimum energy path for NH tautomerization in free-base porphyrin plotted vs the reaction coordinate s in the mass-weighted Cartesian coordinate (see Fig. 4 for labels). N1–N2 distance refers to the distance between two N atoms on which hydrogen migration takes place. This figure is adapted from Ref. [24].

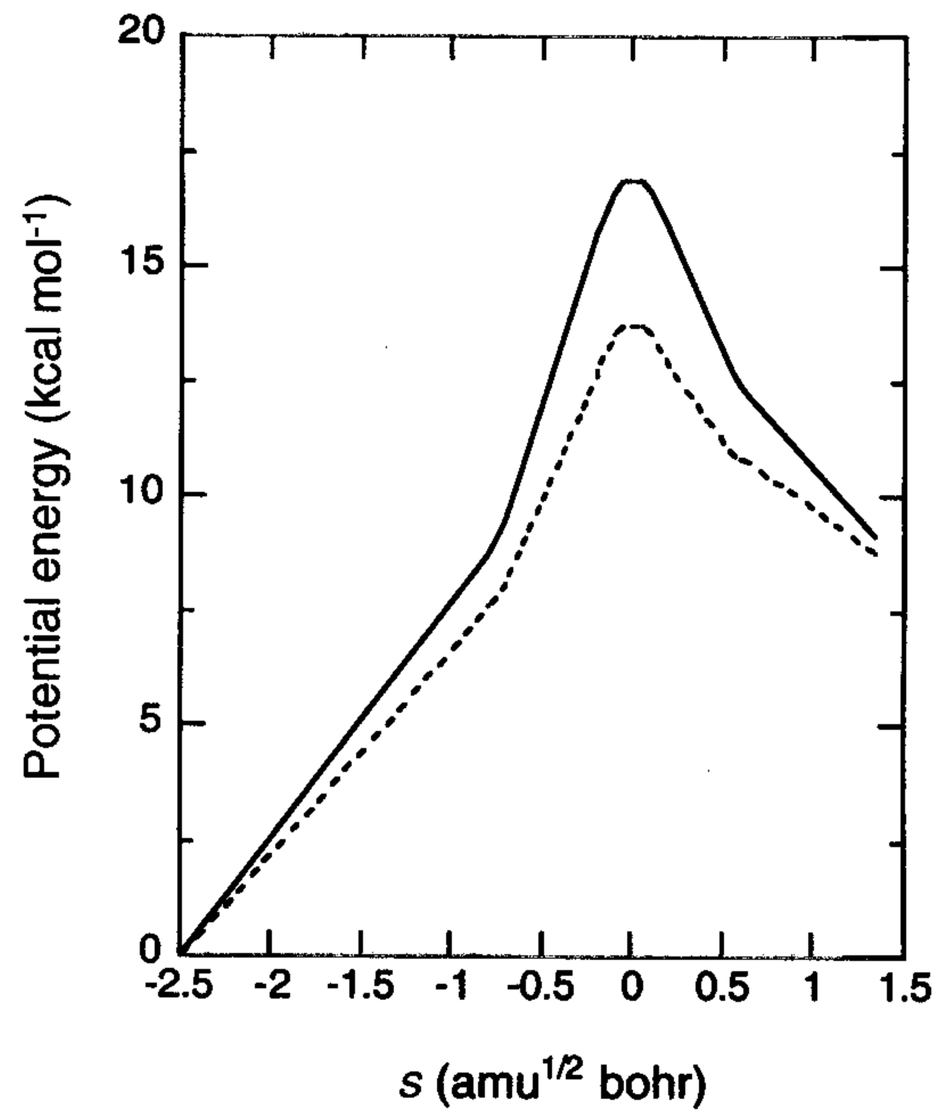

Fig. 7. The classical potential energy $V_{MEP}(s)$ (solid line) and the vibrationally ground-state adiabatic potential energy $V_a^G(s)$ (dashed line) curves along the minimum energy path for NH tautomerism in free-base porphyrin plotted vs the reaction coordinate s in the mass-weighted Cartesian coordinate. This figure is adapted from Ref. [24].

Minimum Energy Path (MEP)

The structural change of porphyrin has been examined as it proceeds from the reactant to the intermediate of the preferred stepwise mechanism [23, 24]. The only significant structural changes that are larger than 2% in the bond length of porphyrin are these of the transferring hydrogen atom. The N–H bond length (r1, as labeled in Fig. 4) of the transferring hydrogen atom is lengthened by +32% to reach the transition state structure (≈1.32 Å) from the reactant structure (≈1.00 Å at −2.55 amu$^{1/2}$ bohr of the MEP). The angle labeled by a1 in Fig. 4 is found to have the largest change of −15.1% to reach the transition state (105.8°) from the reactant structure (124.6°). These active bond lengths and angle essentially relate to the N–H stretching and bending modes which were thought to be responsible for the process of tautomerization in mode-selective vibrational spectroscopic studies [42]. The structural changes vs reaction coordinate can be viewed as the changes in N–N and N–H bond distances respectively, as displayed in Fig. 6. Examination of N–N and N–H bond distance profiles as functions of the reaction coordinate reveals an interesting observation. In particular, the first step of the stepwise tautomerization process in gas-phase free-base porphyrin can be viewed as a two-stage process in which the changes in the structure along the reaction path can be divided into two distinct parts, each involving different types of motions. More specifically, the N–N bond distance between the donor and acceptor nitrogens first compresses approximately from 2.91 to 2.51 Å while the active N–H bond distance (r7 bond in Fig. 4) remains relatively unchanged approximately up to $s = -0.8$ amu$^{1/2}$ bohr from the reactant. At this point, the N–N bond distance stays relatively constant while the hydrogen atom transfers from the donor to the acceptor nitrogen as its bond length is stretched from 1.0 to 1.32 Å to reach the saddle point. One can think of this two-stage process as the porphyrin first going through a global structure compression to bring the donor and acceptor sites closer together so as to lower the barrier for hydrogen atom transfer. Such deformation will reach a point when further compression would outcost the hydrogen atom transfer process. At that point one observes hydrogen atom transfer but with no further global structure compression. Figure 7 depicts the energy cost for global compression to be about 8.7 kcal mol^{-1} (the potential energy value at $s = -0.8$ amu$^{1/2}$ bohr along the MEP). The remaining energy cost of ~8.2 kcal mol^{-1} can be thought of as the barrier to hydrogen atom transfer in the second stage. Such a two-stage process observed here is not unique to this tautomerization process. Similar structural changes were also observed in the concerted double hydrogen atom transfer in formamidine–water and formamide–water complexes [57]. This information could be very useful in designing new porphyrins for material science and biological applications. Previously, there has been some discussion on the structural changes of the skeleton on hydrogen atom migration in the case of monodeprotonated free-base porphyrin based on theoretical [58, 59] and experimental [56, 60] studies. However, the discussion was limited to the differences between the reactant and transition state structures and thus was not able to reveal the two-stage process as discussed above.

KINETICS OF NH TAUTOMERIZATION

Up to date there are only three theoretical studies on the kinetic aspects of this tautomerization process. The first study used the conventional transition state theory (TST) with no tunneling contribution [21] and the second one employed a direct dynamics method with an instanton

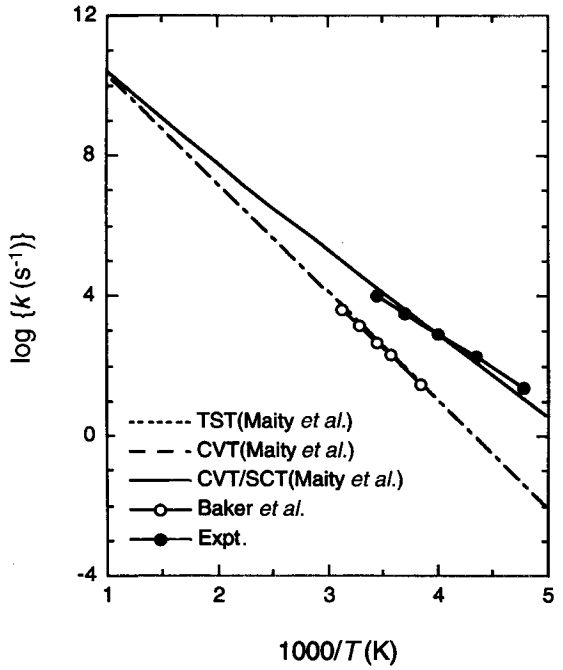

Fig. 8. Comparison of Arrhenius plots of the experimental and calculated forward (*trans*-isomer → *cis*-isomer) rate constants vs 1000/*T* at different levels of theory of rate calculations and tunneling corrections for NH tautomerization in free-base porphyrin. Note that TST and CVT rate profiles are overlaped. The experimental data are generated from the Arrhenius equation as suggested in Ref. [39]. This figure is adapted from Ref. [24].

approach for tunneling corrections [51]. The more recent study applied the canonical variational transition state theory (CVT) with multidimensional semiclassical small-curvature tunneling (SCT) corrections [24]. The theoretical rate calculation performed at the simple TST level of theory without incorporating any tunneling correction is found to be lower by a factor of 60 compared to the available experimental value of $1.8e+3\ s^{-1}$ at 260 K from Braun *et al.* [39]. This factor of 60 has indeed been verified by Maity *et al.* to be mainly due to tunneling contribution. Since both studies [24, 51] using different methods concluded that tunneling effects are significant in this system, it is worthwhile to briefly discuss the differences in these two methods for calculation of tunneling contributions.

Both the SCT and instanton methods require calculations of the action integral over a certain tunneling path. The SCT method assumes the tunneling path to be along the minimum energy path and includes the reaction path curvature effects by using an effective reduced mass. The instanton approach assumes the tunneling path to be the least action path. The correct tunneling path, however, is the one that gives the largest tunneling probability for a given energy. This gives the impression that the least action path would be a better approximation to the correct tunneling path at low temperatures. This, however, assumes certain uniformity in the motion along the tunneling path. From the motion along the minimum energy path discussed above, namely the two-stage process, it is not the case for proton transfer in porphyrin. Both methods use the vibrational adiabatic approximation to treat the transverse modes. The accuracy in calculating the tunneling probability however depends strongly on the vibrational adiabatic potential

Table 7. A comparison of the experimental and calculated energy of activation, E_a in kcal mol^{-1}, for the NH tautomerization process in free-base porphyrin

Method	E_a
Experimental	
Abraham *et al.*[a]	9.2 (308 K)
Eaton and Eaton[b]	9.0–11.4 (298 K)
Braun *et al.*[c]	8.8 (209–309 K)
	9.3 (223–290 K)
Frydman *et al.*[d]	8.3 (110 K)
Butenhoff and Moore[e]	4.8–5.6 (110 K)
Theory (200–300 K)	
TST[f]	13.6
TST[g]	14.1
TST/W[g]	13.3
TST/Eckart[g]	11.1
CVT[g]	14.1
CVT/ZCT[g]	11.6
CVT/SCT[g]	10.8

[a] Ref. [26].
[b] Ref. [27]; this is for tetraaryl porphyrins.
[c] Ref. [39]; the value in the lower line is for the bulk solid.
[d] Ref. [50].
[e] Ref. [41].
[f] Ref. [21].
[g] Ref. [24].

curve. In the instanton calculations, it was adjusted to fit the experimental rate constants for this reaction and its corresponding isotopic substitution ones. Despite such adjustments and minor shortcoming in the calculated kinetic isotope effects, the conclusion on the importance of the tunneling effects is valid [61]. In the SCT calculations, the potential curve for tunneling is calculated from first principles without any readjustment. Thus, the calculated rate constants have more predictive values.

Since the calculated rate constants using the instanton method were not reported [51], we can not make a comparison with the SCT results presented below.

Figure 8 displays the Arrhenius plots of the calculated TST and CVT rate constants for the forward reaction of *trans* ↔ *cis* isomerization in free-base porphyrin in the temperature range of 200–1000 K. The recrossing effect was found to be very small as expected due to the relatively large barrier height. However, tunneling effects were found to be very significant especially in the lower temperature range as indicated by the large curvature of the CVT/SCT (SCT refers to multidimensional small curvature tunneling correction) curve as a function of the temperature and its large deviation from the CVT results. For example, at 200 K, tunneling enhances the transfer rate by a factor of ~4170. The calculated overall transfer rate at CVT/SCT level of theory is in excellent agreement with the experimental data. The non-Arrhenius equation for the forward NH tautomerization process is suggested to be

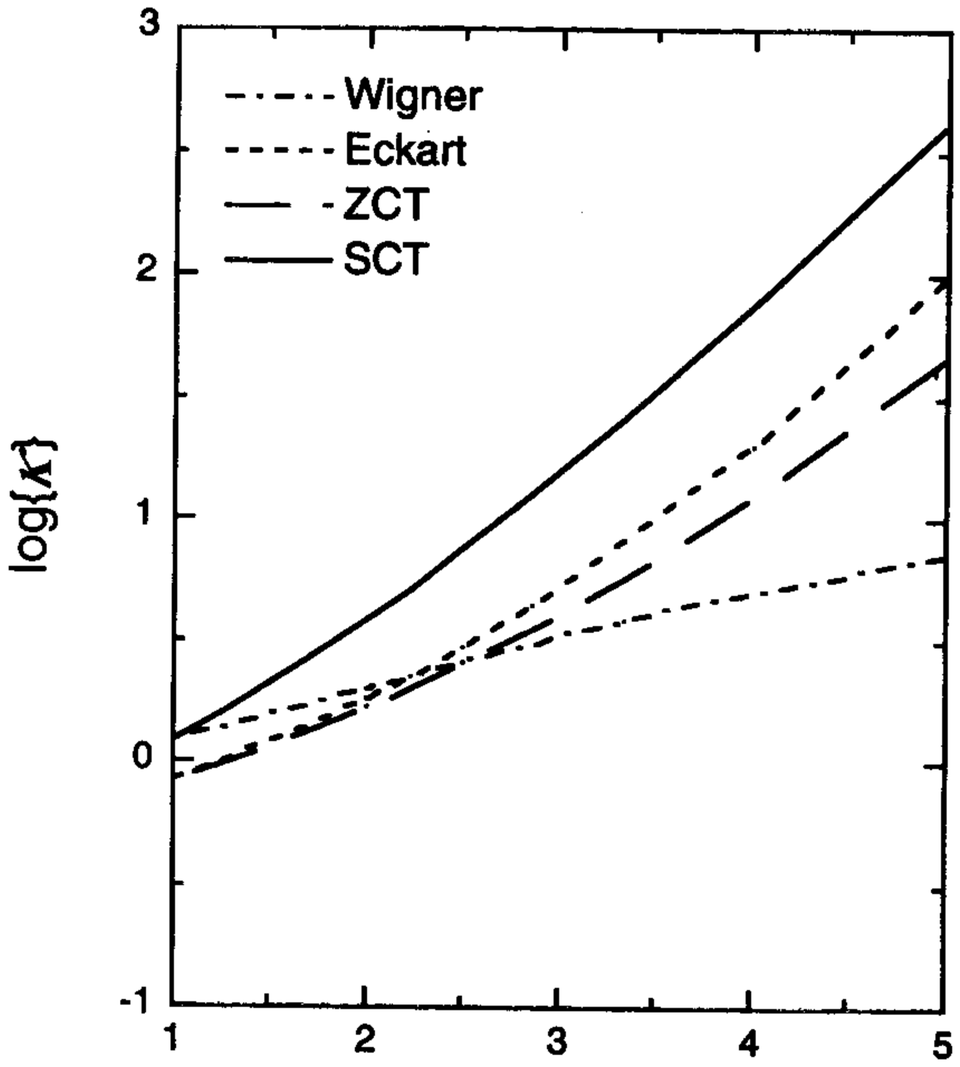

Fig. 9. Log plot of calculated transmission coefficient (κ) vs $1000/T$ at different levels of tunneling corrections for the forward NH tautomerization process in free-base porphyrin. SCT and ZCT stand for small curvature tunneling and zero curvature tunneling corrections, respectively. This figure is adapted from Ref. [24].

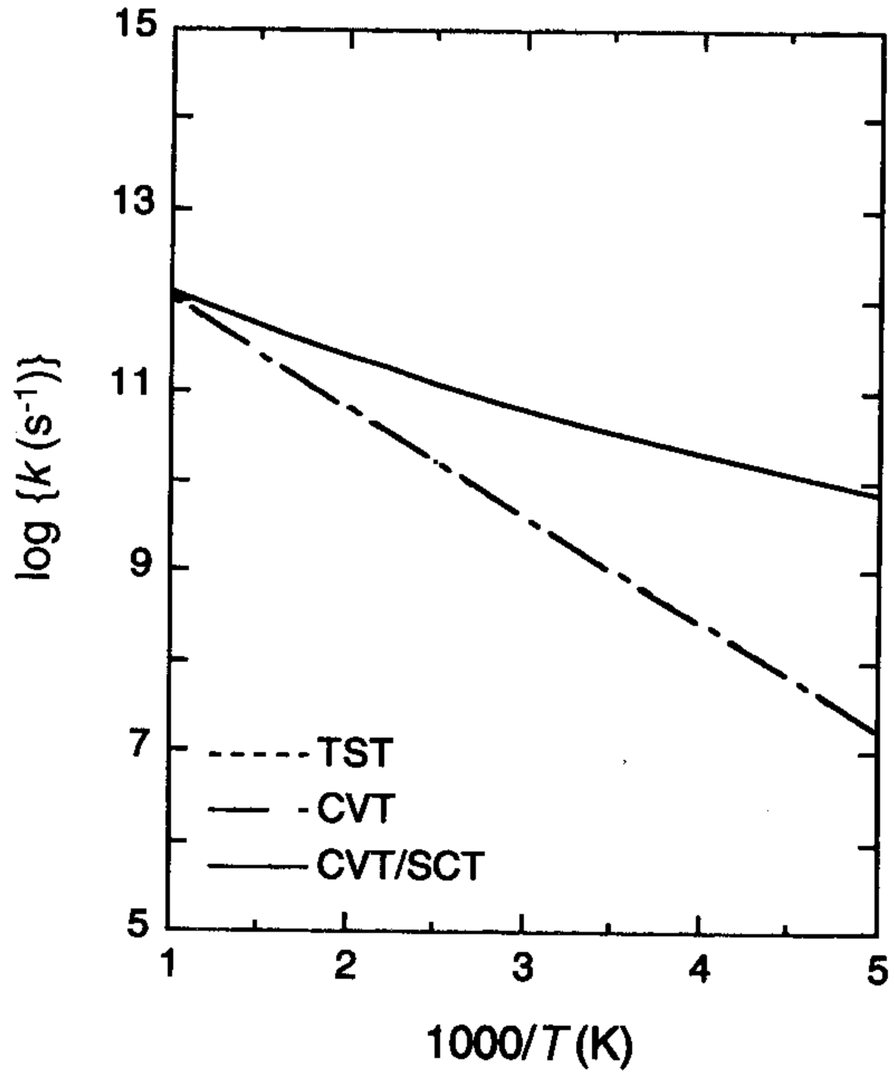

Fig. 10. Arrhenius plots of the calculated reverse rate constants vs $1000/T$ at different levels of theory of rate calculations and tunneling corrections for NH tautomerization in free-base porphyrin. Note that TST and CVT rate profiles are overlaped. This figure is adapted from Ref. [24].

$k(\mathrm{s}^{-1}) = 5.05\mathrm{e}+08 \times T^{1.29} \exp(-9.9\,\mathrm{kcal\ mol}^{-1}/RT)$ in the temperature range of 200–1000 K.

Calculated activation energies (E_a) in the temperature range of 200–300 K for NH tautomerization along with available experimental data are listed in Table 7. The most accurate theoretical prediction to date for the activation energy (CVT/SCT value of 10.8 kcal mol^{-1}) is within the range of experimental data provided by Eaton and co-workers [27] and higher than that the experimental data provided by Braun and co-workers [39] from their NMR line shapes and a modified Bell-tunneling model. The experimental activation energy of 4.8–5.6 kcal mol^{-1} at 110 K provided by Butenhoff and Moore from their laser-induced fluorescence spectroscopy and a one-dimensional Eckart tunneling model is much lower than the present calculated as well as other experimental data from Frydman *et al.* [49]. Note that the activation energies from TST calculations without tunneling corrections reported by both studies differ from each other by only 0.5 kcal mol^{-1} and are too large compared to the experimental data. When tunneling corrections are included, the calculated E_a improves as more accurate tunneling methods were employed.

Due to the importance of tunneling in this process, it is worth discussing the performance of different tunneling approximations that have been considered. Figure 9 displays the calculated transmission coefficient (κ) as functions of the temperature using different tunneling models. The SCT method is the most accurate approximation used to date and thus we used it as a reference point for comparison. First of all, the Wigner model as expected greatly underestimates the tunneling contribution since it assumes tunneling to occur at the top of the barrier and is reasonable only at moderate to high temperatures. Even though the Eckart model requires additional potential information at the intermediate stage beyond those needed for the TST calculation, it predicts a much more accurate tunneling contribution than the Wigner model. Recall that in the Eckart model, the vibrationally ground-state adiabatic potential energy curve for tunneling is approximated by a one-dimensional Eckart function. In other words, it is an approximation to the ZCT (multidimensional zero curvature tunneling correction) method. A remarkable agreement between the Eckart model and the ZCT method indicates the potential curve along the MEP can be well represented by an Eckart function. The results suggest that the Eckart tunneling model should be used in experimental analysis as done by Butenhoff and Moore, instead of the Bell model. Finally, comparing the ZCT and SCT results, it is found that the 'corner cutting' effect accounts for nearly an order of magnitude increase in the rate for temperature below 300 K.

Figure 10 depicts the Arrhenius plot of the calculated results for the reverse NH tautomerization process which is essentially the second step of the two-step intra-molecular hydrogen atom transfer process. Similar to the forward reaction, recrossing effect was also found to be very small. However, noticeably larger tunneling effects are found in the lower temperature range. The activation energy (E_a) for this process was calculated to be 2.1 kcal mol^{-1} in the temperature range of 200–300 K from the present CVT rate calculation incorporating multi-dimensional semiclassical SCT tunneling corrections. The non-Arrhenius equation for the reverse NH tautomerization process (the second step of the process) in free-base porphyrin is suggested to be $k(\mathrm{s}^{-1}) = 9.71\mathrm{e}+08 \times T^{1.17} \exp(-1.7\,\mathrm{kcal\ mol}^{-1}/RT)$ over the temperature range from 200 to 1000 K. Previously there has been some discussion regarding the life time of the *cis*-isomer, as to whether it can be experimentally detected. According to this CVT/SCT data for *cis–trans* conversion, the life time of the *cis*-isomer is calculated to be ~25 ps.

This is substantially shorter than the previous estimation of 1–10 ns [21, 56]. However, both the previous results are based on methods not applying any appropriate tunneling corrections. So, the calculated life time of 25 ps for the *cis*-isomer from the CVT/SCT method would be more reasonable.

CONCLUSIONS

This review provides an account on the current status of theoretical modeling of NH tautomerization in free-base porphyrin. Regarding the mechanism, theoretical predictions on the structure and IR spectra of the stable isomer, solvent effects on the tautomerization rate, and the preferred double hydrogen atom migration pathway are in agreement with recent experimental data. In particular, solvent effects were found to be relatively small. The tautomerization proceeds via a step-wise process with a stable intermediate. Furthermore, a global deformation of the porphyrin structure was predicted prior to the hydrogen migration process. Kinetic studies so far are only at the beginning. With the use of a relatively accurate dynamical theory, namely the variational transition state theory augmented with multidimensional semiclassical tunneling corrections, excellent agreement was obtained for the tautomerization rate and activation energy for temperatures above 200 K. However, there remain many challenging problems. For instance, experimental data for HH/HD/DD kinetic isotope effects posed an interesting question regarding validity of the rule of the geometric mean which would require a detailed analysis from accurate kinetic studies.

Acknowledgements

This work is supported by the National Science Foundation. An allocation of computer time from the University of Utah Center for High Performance Computing is gratefully acknowledged.

REFERENCES

1. Dolphin D. (ed). *The Porphyrins*, vol. 1–7. Academic Press; New York, 1978/1979.
2. Leznoff CC, Lever ABP. (eds). *Phthalocynines. Properties and Applications*; vol. 1–3, VCH, Weinheim, 1989–1993.
3. Andreoni A, Cubeddo R. (eds). *Porphyrins in Tumor Phototherapy*, Plenum, New York, 1984.
4. Li X-Y, Zgierski MZ. *J. Phys Chem.* 1991; **95**: 4268.
5. Almlöf J. *Int. J. Quantum Chem.* 1974; **8**: 915.
6. Limbach H-H, Hennig J. *J. Chem. Phys.* 1979; **71**: 3120.
7. Sarai A. *J. Chem. Phys.* 1984; **80**: 5341.
8. Kuzmitsky VA, Solovyov KN. *J. Mol. Struct.* 1980; **65**: 219.
9. Sarai A. *Chem. Phys. Lett.* 1981; **83**: 50.
10. Sarai A. *J. Chem. Phys.* 1982; **76**: 5554.
11. Merz KMJ, Reynolds CH. *J. Chem. Soc., Chem. Commun.* 1988; 90.
12. Smedarchina Z, Siebrand W, Wildman TA. *Chem. Phys. Lett.* 1988; **143**: 395.
13. Almlöf J, Fischer TH, Gassman PG, Ghosh A, Häser M. *J. Phys. Chem.* 1993; **97**: 10 964.
14. Ghosh A, Almlöf J. *Chem. Phys. Lett.* 1993; **213**: 519.
15. Ghosh A. *J. Phys. Chem.* 1994; **98**: 11 004.
16. Merchán M, Ortí E, Roos BO. *Chem. Phys. Lett.* 1994; **221**: 136.
17. Reimers JR, Lü TX, Crossley MJ, Hush NS. *J. Am. Chem. Soc.* 1995; **117**: 2855.
18. Ghosh A, Almlöf J. *J. Phys. Chem.* 1995; **99**: 1073.
19. Kozlowski PM, Zgierski MZ, Pulay P. *Chem. Phys. Lett.* 1995; **247**: 379.
20. Kozlowski PM, Jarzecki AA, Pulay P. *J. Phys. Chem.* 1996; **100**: 7007.
21. Baker J, Kozlowski PM, Jarzecki AA, Pulay P. *Theor. Chem. Acc.* 1997; **97**: 59.
22. Wu Y, Chan KWK, Yip C, Vogel E, Plattner DA, Houk KN. *J. Org. Chem.* 1997; **62**: 9240.
23. Maity DK, Bell RL, Truong TN. In 217th ACS National Meeting Anaheim, CA, 1999.
24. Maity DK, Bell RL, Truong TN. *J. Am. Chem. Soc.* 2000; **122**: 897.
25. Chen BML, Tulinsky A. *J. Am. Chem. Soc.* 1972; **94**: 4144.
26. Abraham RJ, Hawkes GE, Smith KM. *Tetrahedron Lett.* 1974; **16**: 1483.
27. Eaton SS, Eaton GR. *J. Am. Chem. Soc.* 1977; **99**: 1601.
28. Hennig J, Limbach H-H. *J. Chem. Soc., Faraday Trans. 2* 1979; **75**: 752.
29. Limbach H-H, Hennig J, Gerritzen D, Rumpel H. *Faraday Dis. Chem. Soc.* 1982; **74**: 229.
30. Hennig J, Limbach H-H. *J. Magn. Reson.* 1982; **49**: 322.
31. Hennig J, Limbach H-H. *J. Am. Chem. Soc.* 1984; **106**: 292.
32. Limbach H-H, Hennig J, Kendrick R, Yannov CS. *J. Am. Chem. Soc.* 1984; **106**: 4059.
33. Crossley MJ, Harding MM, Sternhell S. *J. Am. Chem. Soc.* 1986; **108**: 3608.
34. Schlabach M, Wehrle B, Limbach H-H, Bunnenberg E, Knierzinger A, Shu AYL, Tolf BR, Djerassi C. *J. Am. Chem. Soc.* 1986; **108**: 3856.
35. Stilbs P, Moseley ME. *J. Chem. Soc., Faraday Trans. 2* 1980; **76**: 731.
36. Stilbs P. *J. Magn. Reson.* 1984; **58**: 152.
37. Schlabach M, Scherer G, Limbach H-H. *J. Am. Chem. Soc.* 1991; **113**: 3550.
38. Braun J, Schlabach M, Wehrle B, Köcher M, Vogel E, Limbach H-H. *J. Am. Chem. Soc.* 1994; **116**: 6593.
39. Braun J, Limbach H-H, Williams PG, Morimoto H, Wemmer DE. *J. Am. Chem. Soc.* 1996; **118**: 723.
40. Limbach H-H, Hennig J, Stulz J. *J. Chem. Phys.* 1983; **78**: 5432.
41. Butenhoff TJ, Moore CB. *J. Am. Chem. Soc.* 1988; **110**: 8336.
42. Butenhoff TJ, Chuck RS, Limbach H-H, Moore CB. *J. Phys. Chem.* 1990; **94**: 7847.
43. Spiro TG. *Adv. Protein Chem.* 1985; **37**: 111.
44. Yu N. *Methods Enzymol.* 1986; **130**: 350.
45. Spiro TG. (ed). *Biological Applications of Raman Spectroscopy*; vol. 3., Wiley Interscience, New York, 1988.
46. Radziszewski JG, Waluk J, Michl J. *Chem. Phys.* 1989; **136**: 165.
47. Radziszewski JG, Waluk J, Michl J. *J. Mol. Spectrosc.* 1990; **140**: 373.
48. Webb LE, Fleischer EB. *J. Chem. Phys.* 1965; **43**: 3100.
49. Frydman L, Olivieri AC, Diaz LE, Frydman B, Morin FG, Mayne CL, Grant DM, Adler AD. *J. Am. Chem. Soc.* 1988; **110**: 336.
50. Crossley MJ, Harding MM, Sternhell S. *J. Am. Chem. Soc.* 1992; **114**: 3266.

51. Smedarchina Z, Zgierski MZ, Siebrand W, Kozlowski PM. *J. Chem. Phys.* 1998; **109**: 1014.
52. Reynolds CH. *J. Org. Chem.* 1988; **53**: 6061.
53. Hammond GS. *J. Am. Chem. Soc.* 1955; **77**: 334.
54. Svensson M, Humbel S, Froese RDJ, Matsubara T, Sieber S, Morokuma K. *J. Phys. Chem.* 1996; **100**: 19 357.
55. Cossi M, Barone V, Cammi R, Tomasi J. *Chem. Phys. Lett.* 1996; **255**: 327.
56. Braun J, Hasenfratz C, Schwesinger R, Limbach H. *Angew. Chem. Int. Ed. Engl.* 1994; **33**: 2215.
57. Bell RL, Truong TN. *J. Chem. Phys.* 1994; **101**: 10 442.
58. Vangberg T, Ghosh A. *J. Phys. Chem. B* 1997; **101**: 1496.
59. Brackhagen O, Scheurer C, Meyer R, Limbach H. *Ber. Bunsenges. Phys. Chem.* 1998; **102**: 303.
60. Braun J, Schwesinger R, Williams PG, Morimoto H, Wemmer DE, Limbach H-H. *J. Am. Chem. Soc.* 1996; **118**: 11 101–11 110.
61. Siebrand W, Smedarchina Z, Zgierski M, Fernandez-Ramos A. *Int. Rev. Phys. Chem.* 1999; **18**: 5.